REPORT DOCUMENTATION PAGE

Form Approved
OMB NO. 0704-0188

1. AGENCY USE ONLY (Leave Blank)	2. REPORT DATE	3. REPORT TYPE AND DATES COVERED
		reprint, FY2007

4. TITLE AND SUBTITLE
Local bonding analysis of the valence and conduction band features of TiO2

5. FUNDING NUMBERS
W911NF-04-D-0003

6. AUTHOR(S)
L. Fleming, C. C. Fulton, G. Lucovsky, J. E. Rowe, M. D. Ulrich, J. Luning

7. PERFORMING ORGANIZATION NAME(S) AND ADDRESS(ES)
Dept of Physics, NCSU, Raleigh, NCS 27695-8202

8. PERFORMING ORGANIZATION REPORT NUMBER

9. SPONSORING / MONITORING AGENCY NAME(S) AND ADDRESS(ES)
U. S. Army Research Office
P.O. Box 12211
Research Triangle Park, NC 27709-2211

10. SPONSORING / MONITORING AGENCY REPORT NUMBER
48745.7-PH-SR

11. SUPPLEMENTARY NOTES
The views, opinions and/or findings contained in this report are those of the author(s) and should not be construed as an official Department of the Army position, policy or decision, unless so designated by other documentation.

12 a. DISTRIBUTION / AVAILABILITY STATEMENT
Approved for public release; Federal Purpose Rights.

12 b. DISTRIBUTION CODE

13. ABSTRACT (Maximum 200 words)

An analysis of the valence and conduction band electronic structure of TiO2 as studied by ultraviolet photoemission spectroscopy UPS and x-ray absorption spectroscopy XAS using synchrotron radiation is reported. Valence band spectra from UPS have been deconvolved using a five-peak model. The spectra are interpreted based on the peak assignments to the XAS data and the symmetries of the valence band states. The interpretation is consistent with theoretical calculations of molecular orbitals found in the literature. The removal of the d-state degeneracies that arise from a collective Jahn–Teller splitting of the crystal field split t2g and eg states is observed and scales with the conduction band results from the absorption data. These Jahn–Teller derived energy separations are present in the O K1 and Ti L3 spectra but are not resolved in the photoemission valence band spectra. Two defect states are clearly observed 0.7 and 2.0 eV above the valence band edge and are attributed to the presence of oxygen atom vacancies that are described in terms of Ti3+ states.

14. SUBJECT TERMS
oxides, spectroscopy, electronic structure, gate dielectric

15. NUMBER OF PAGES
7

16. PRICE CODE

17. SECURITY CLASSIFICATION OR REPORT	18. SECURITY CLASSIFICATION ON THIS PAGE	19. SECURITY CLASSIFICATION OF ABSTRACT	20. LIMITATION OF ABSTRACT
UNCLASSIFIED	**UNCLASSIFIED**	**UNCLASSIFIED**	**UU**

NSN 7540-01-280-5500

Standard Form 298 (Rev.2-89)
Prescribed by ANSI Std. 239-18
298-102

Enclosure 1

Local bonding analysis of the valence and conduction band features of TiO_2

L. Fleming,[a] C. C. Fulton, G. Lucovsky, and J. E. Rowe
Department of Physics, North Carolina State University, Raleigh, North Carolina 27695-8202

M. D. Ulrich
Army Research Office, Physics Division, Research Triangle Park, North Carolina 27709-2211
and Department of Physics, North Carolina State University, Raleigh, North Carolina 27695-8202

J. Lüning
Stanford Synchrotron Radiation Laboratory, Stanford University, Menlo Park, California

(Received 8 March 2007; accepted 13 June 2007; published online 7 August 2007)

An analysis of the valence and conduction band electronic structure of TiO_2 as studied by ultraviolet photoemission spectroscopy (UPS) and x-ray absorption spectroscopy (XAS) using synchrotron radiation is reported. Valence band spectra from UPS have been deconvolved using a five-peak model. The spectra are interpreted based on the peak assignments to the XAS data and the symmetries of the valence band states. The interpretation is consistent with theoretical calculations of molecular orbitals found in the literature. The removal of the *d*-state degeneracies that arise from a collective Jahn–Teller splitting of the crystal field split t_{2g} and e_g states is observed and scales with the conduction band results from the absorption data. These Jahn–Teller derived energy separations are present in the O K_1 and Ti L_3 spectra but are not resolved in the photoemission valence band spectra. Two defect states are clearly observed ~0.7 and 2.0 eV above the valence band edge and are attributed to the presence of oxygen atom vacancies that are described in terms of Ti^{3+} states.
 [DOI: 10.1063/1.2764004]

I. INTRODUCTION

The electronic structure of TiO_2 has been widely studied due to its importance as an industrial catalyst in thermal or photoinduced chemical reactions.[1,2] Thorough reviews of the surface properties and electronic structure of TiO_2 are available in the literature.[3,4] Many studies have employed single crystals of TiO_2 and controlled ion bombardment or oxidation to characterize surface structure and defects.[5–7] Results have generally been interpreted within an extended picture incorporating the bulk and surface band structures. More recently, interest in the inclusion of TiO_2 and other group IVB transition metal oxides (ZrO_2, HfO_2) in high-dielectric-constant ("high-*k*") gate stacks for advanced metal oxide semiconductor field effect transistors (MOSFETs) has made it useful to revisit these material systems. These applications require deposited films, which are generally nanocrystalline in character. Hence, an understanding of the local bonding in these oxides, including grain boundary formation, defect behavior, and scales of order, is essential to the successful implementation of high-*k* devices.

TiO_2 has a very high κ value[8] of 50–80 but is thermally unstable on Si, where it reacts to form SiO_2, Ti_xO_y, and possibly Ti silicide phases.[9] In addition, the polycrystalline habit of many transition metal oxides can create leakage paths during device operation. Transmission electron microscopy of group IVB transition metal (TM) oxide films deposited by remote plasma-enhanced chemical vapor deposition or reactive evaporation has revealed nanocrystallinity with grain sizes of approximately 2 nm.[10] X-ray diffraction cannot detect order on this scale. While none of the group IVB oxides provides an independent solution for advanced MOSFET gate dielectrics, the research on alloys of these materials with other oxides is still in an early phase and remains promising. Silicon oxynitride alloys containing Hf and Ti have recently been shown[11] to suppress the phase separation that occurs under standard processing temperatures in the silicate alloys of group IVB transition metals.[12,13]

Before the value of TM oxides or their alloys for MOSFET applications can be justified, an understanding of the physical and electronic structure of the constituent members must be developed. Though the physical[14–16] and electronic properties[5–7,17–19] of TiO_2 have been the subject of previous studies, the resolution offered by the present studies reveals the local physical origin of the electronic structure in nanocrystalline films. TiO_2 has further been chosen as a natural starting point to understand other TM oxides of interest to the MOSFET community. In this article, we study the valence and conduction band electronic properties of TiO_2 using ultraviolet photoemission spectroscopy (UPS) and x-ray absorption spectroscopy (XAS) and interpret our experimental results with molecular orbital theory.

II. EXPERIMENTAL

The samples were prepared from heavily doped *n*-type Si (100) substrates of 25 mm diameter. The substrates were introduced directly into a molecular beam deposition (MBD) system under ultrahigh-vacuum (UHV) conditions, without removal of the native oxide. Growth of the transition metal

[a]Electronic mail: lbflemin@unity.ncsu.edu

oxide (Ti) was accomplished by simultaneous electron-beam evaporation of the titanium onto the substrates in an atmosphere of 2×10^{-6} Torr of O_2. The metal deposition rate was monitored using a Sycon Instruments STM-100 crystal monitor located close to the evaporation source. A shutter was used to control the onset and exposure time of the substrates to the evaporating metal. Oxide film thickness was determined from the molar density of the metal and metal oxide, and the measured deposition rate and exposure time. Assuming that the film undergoes complete oxidation, the oxide-to-metal thickness ratio is 2:1 for TiO_2. This assumption has been verified by XPS studies of the substrate Si 2*p* core-level spectra with film thickness. The oxide films used in this study were approximately 50 Å thick. Initial *in-situ* x-ray photoelectron spectroscopy was used to confirm the TiO_2 composition.

After growth of the films, the substrates were split in two, with one half undergoing annealing at 800 °C. Another set of samples, annealed at 900 °C, were prepared for x-ray absorption studies (XAS). All samples were transported in air from the growth, processing, and characterization system to separate facilities for XAS and ultraviolet photoemission spectroscopy (UPS). The XAS measurements were performed at the 10–1 beamline of the Stanford Synchrotron Research Laboratory (SSRL) at the Stanford Linear Accelerator Center (SLAC). This beamline features a spherical grating monochromator and a wiggler source. The slit widths were set to give a resolution of 100 meV at 500 eV photon energy. All measurements employed a total photoelectron yield approach to measure the absorption by recording the sample drain current. Photon flux was similarly determined by measuring the total electron yield from an 80% transmissive gold grid. To correct for energy shifts of the monochromator, a reference sample containing a series of oxidized 3*d* transition metals was measured in parallel with that of the TiO_2 sample.

In previous papers, the abbreviation SXPS, for soft XPS, has been applied to valence band spectra similar to those shown in this paper. However, the term UPS is used here because of the relatively low photon energies. The UPS measurements were performed at the U4A beamline of the National Synchrotron Light Source. This beamline is equipped with a set of spherical grating monochromators which produce a tunable photon beam of 10–250 eV. Photoelectron kinetic energies were measured using a VSW 100 mm hemispherical analyzer operating at a fixed 45° angle to the photon beam axis, and in fixed pass energy mode. Spectra were acquired in normal emission geometry (90° take-off angle). The beamline and analyzer were set up to give an instrumental resolution of 0.17 eV. Because of the surface sensitivity of UPS, each sample was degassed by heating to ~200 °C to remove surface adsorbates, primarily water. Valence band spectra were obtained for each sample at photon energies of 40 eV and 60 eV. Si 2*p* core level spectra were measured for each sample with a photon energy of 150 eV to determine if Si was incorporated into the film. For each change of the photon energy, a reference Fermi energy was measured on a gold sample attached to the same sample mount. The exact photon energy was confirmed by measuring this reference with both first- and second-order light.

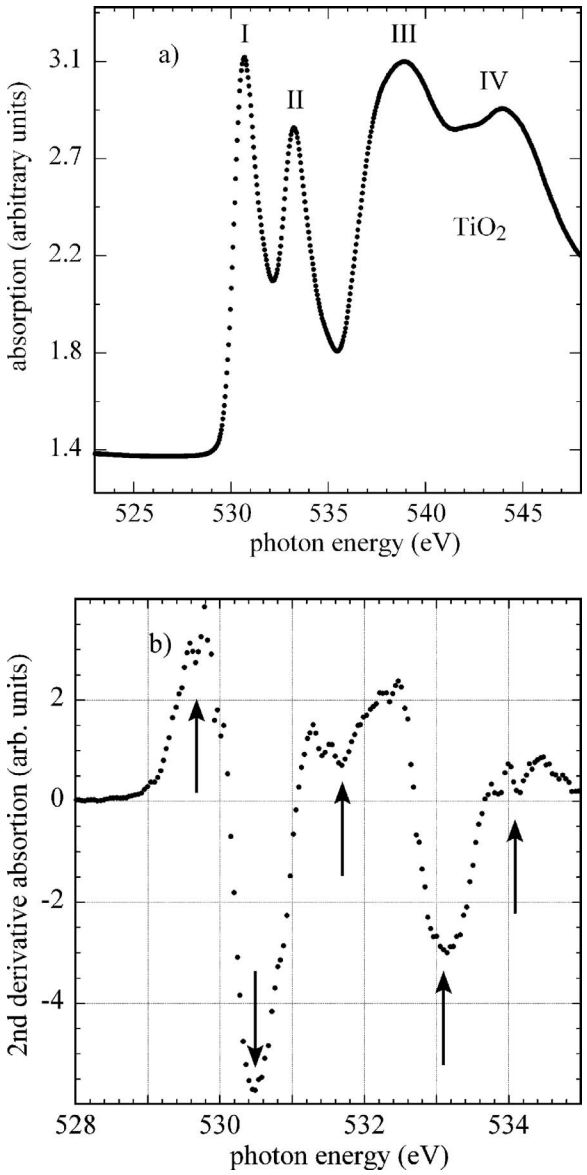

FIG. 1. (a) O K_1 XAS data for TiO_2. (b) O K_1 second derivative spectra of TiO_2. Arrows indicate Jahn–Teller split states.

III. RESULTS

A. XAS results

Shown in Fig. 1 is the O K_1 XAS spectrum for TiO_2 annealed at 900 °C. Four main features can be seen in addition to the edge at 529 eV. The O K_1 (more often simply referred to the O *K* spectrum) involves transition from the O 1*s* core state to molecular orbital (MO) states of the TiO_2 nanocrystallites, O 2*p* anti-bonding states. Since these are MO states of the crystal, they also include spectral features that reflect the mixing of the Ti 3*d*, 4*s*, and 4*p* states, because states with these symmetries also comprise the valence band bonding states.[20] The O K_1 spectrum includes two distinct and relatively sharp peaks located at 530.5 eV and 533.1 eV, labeled I and II, that are associated with Ti 3*d* states, and two

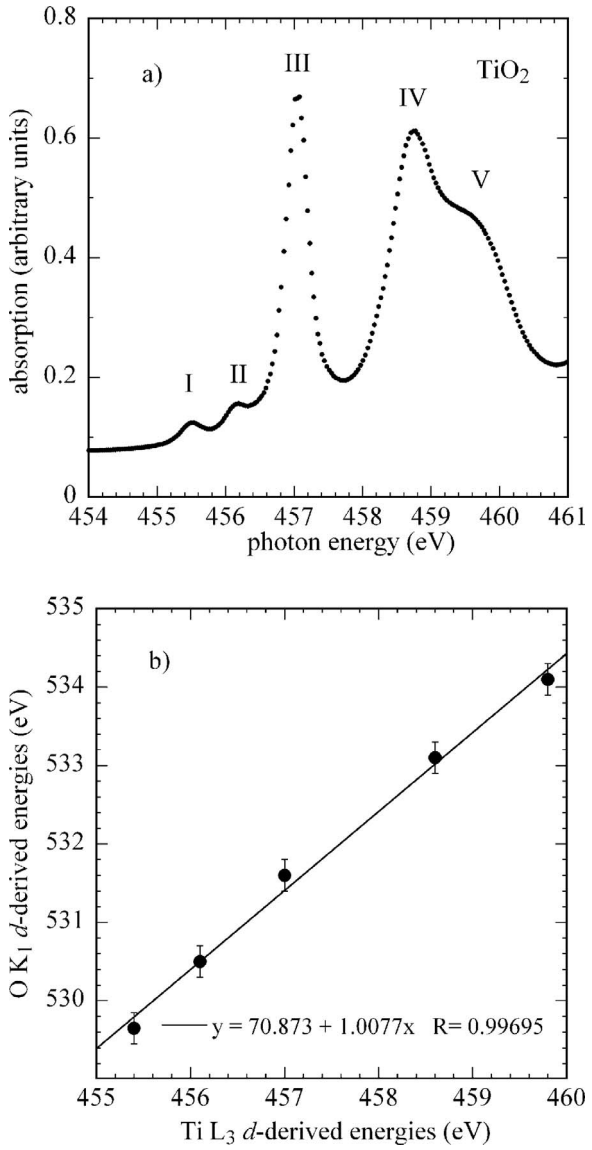

FIG. 2. (a) L_3 spectrum of TiO_2. (b) Plot of the O K_1-derived features versus the Ti L_3 peaks.

broad features at about 539 eV and 544 eV labeled III and IV that are associated with Ti 4*s* and 4*p* states. Though peaks I and II are relatively sharp, they are also noticeably asymmetric. The second derivative of the spectrum, shown in Fig. 1(b), reveals that these two peaks are comprised of five underlying features at 529.65 eV, 530.5 eV, 531.6 eV, 533.1 eV, and 534.1 eV. In Fig. 2(a), the Ti L_3 spectrum of TiO_2 is shown. The transitions in the L_3 spectrum are from the Ti $2p_{3/2}$ spin orbit split states to Ti $3d$ t_{2g} and e_g final states which display Jahn–Teller splittings. Five features are distinguishable. The peaks, labeled I through V, are at 455.4 eV, 456.10 eV, 457.0 eV, 458.6 eV, and 459.8 eV. A plot of the O K_1 spectrum energies of the five features comprising peaks I and II versus the Ti L_3 spectrum energies for peaks I through V is given in Fig. 2(b). The plot is linear and has a slope of unity.

B. UPS studies

The silicon content of the TiO_2 samples was estimated at less than 2% based on initial *in-situ* XPS characterization,

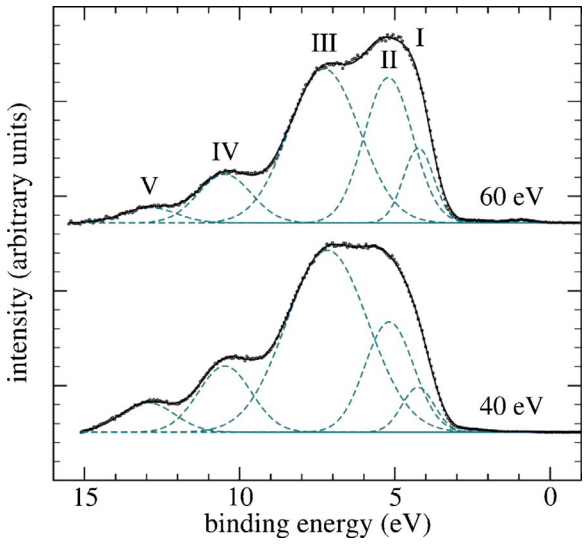

FIG. 3. Ultraviolet photoelectron valence band spectra of TiO_2 at 60 eV and 40 eV photon energies. Five peaks are shown from fits to the data.

indicating that the films were thick enough to avoid significant substrate or native substrate oxide contributions to the data. They were also thin enough to avoid significant charging problems when exposed to the higher photon flux available at the synchrotron. A systematic change of the photon flux by two orders of magnitude revealed a shift of less than 0.1 eV in the measured photoelectron kinetic energy. This is consistent with previous studies of similar oxides at U4A that have shown negligible charging for films below ~75 Å.[21]

Shown in Fig. 3 are the valence band spectra obtained from UPS at 60 eV and 40 eV photon energies. The spectra have been normalized by height and referenced to the Fermi level of the gold reference sample. The valence band data have been fit using a model of five Gaussian peaks, as discussed below. A simple background of the form $a+cx^d$ was used in the fits and has been subtracted from the spectra. The five-peak model for fitting the valence band region of the spectra was chosen based on the expected contributions from

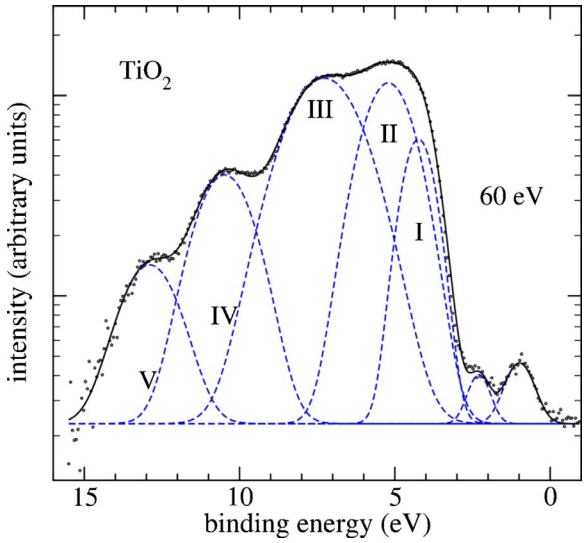

FIG. 4. UPS valence band spectra of TiO_2 on a logarithmic scale. Two defect peaks are observed above the valence band edge.

TABLE I. Binding energy of valence band peaks and band edge. Δd is the separation between peaks II and III.

$h\nu$	Peak I (eV)	Peak II (eV)	Peak III (eV)	Peak IV (eV)	Peak V (eV)	Edge (eV)	Δd
60 eV	4.24	5.21	7.28	10.48	12.89	3.02	2.07
40 eV	4.25	5.18	7.17	10.48	12.96	2.93	1.99

the molecular orbitals that comprise the valence bonding states.[20] The model was also justified for empirical reasons; for example, use of a four-peak model does not adequately fit the valence band edge, and a six-peak model does not further improve the quality of the fits. Though barely discernable to the eye in Fig. 3, a log plot of the spectra (Fig. 4) unambiguously reveals two additional peaks above the valence band edge. Thus, the full model for fitting the spectra employed a seven-peak fit to these data. To maintain a physically relevant model of the data, an excess of free parameters must be avoided. An iterative fitting procedure was thus adopted. The spectra were first fit using a full seven-peak model (five for the valence band and two above the band edge) while allowing the parameters to adjust freely. Following this step, the peaks in the valence band were fixed while the two peaks above the edge were fit separately, limiting the range of the fits to this region. Finally, these two peaks were held constant, and the valence band portion of the spectra was refit. The background exponent was also fixed, based on information gathered from fits of these two spectra and from fits of alloys of TiO_2 and HfO_2.[22]

Results of the fits are given in Tables I and II. All binding energies are given with respect to the Fermi level. Though the presence of electronically active band gap bonding defect states near the valence band edge prevent an exact determination of the edge and offset positions, the approximate position of the valence band edge is given for comparison with other studies. This value was determined as the binding energy at which the intensity of the highest valence band peak has risen to 3% above the baseline after the defect states were subtracted. A quantitatively similar technique is used by Sayan *et al.*[23] In previous studies, similarly doped silicon substrates with a native oxide film have been found to have a valence band maximum at 0.85 eV below the Fermi level. This corresponds to a flatband condition and would give a valence band offset of 2.13 eV for TiO_2. The conduction band offset, based on an E_g estimate of 3.2 eV for TiO_2 (anatase), is therefore $\sim$0 eV. This extrapolated value for TiO_2 is also in agreement with previous measurements.[24] The positions of the defect peaks, at 1.0 eV and 2.3 eV below the Fermi level, respectively, have not been included in the table. Peak areas normalized to the photon flux are displayed in Table II. The most noticeable result is the increase in the peak intensities for the spectra acquired at 40 eV compared to those acquired at 60 eV. This is expected based on the increase in the photoemission cross sections of the Ti 3*d* and O 2*p* atomic levels.[25] The agreement is solely qualitative since cross sections of the molecular orbitals are inherently different from the contributing atomic photoemission cross sections. Slight differences in the relative peak intensities are also observed, as seen in the normalized spectra of Fig. 3. Compared to peak III, the intensities of peaks I and II increase and the intensities of peaks IV and V decrease when the incident photon energy is changed from 40 eV to 60 eV.

A fit of the 800 °C annealed TiO_2 sample data acquired at 60 eV photon energy is given in Fig. 5. The model used to fit the spectra from the as-grown film was inadequate for the annealed sample. An additional peak was necessary in the region corresponding to peak III of Figs. 3 and 4. This correspondence has been highlighted by showing the sum of the two peaks, which appears as a bold line in Fig. 5. An iterative fitting procedure similar to the one described above was also employed in this fit to maintain a physically relevant model of the data.

IV. DISCUSSION

Chemical bonding in transition metal oxides is well-described by molecular orbital theory.[20,26] Local electronic structure associated with *d*-state contributions close to the valence and conduction band edges dominates over the effects of periodicity in determining many electronic and optical properties. Hybridization among the outer *s*, *p*, and *d* atomic orbitals of the metal atoms allows σ and π molecular orbitals to form with the O 2*p* levels. Crystal field splitting separates the TM *d* states into a triply degenerate state of t_{2g} symmetry and a doubly degenerate state of e_g symmetry.[20] Jahn–Teller effects remove the degeneracy of the TM *d* states, giving the valence and conduction bands their rich structure.[26] In TiO_2, the Ti atoms form distorted octahedra (sixfold coordination) with the oxygen atoms and display a high degree of covalency in their bonding.[27] Due to the crystal field splitting in the octahedral symmetry, the e_g states are σ-bonded and are at deeper binding energy among the bonding molecular orbitals of the valence band, and at higher energy among the antibonding molecular orbitals of the con-

TABLE II. Areas and widths of peaks I through V.

$h\nu$		Peak I	Peak II	Peak III	Peak IV	Peak V
60 eV	Area	0.158	0.485	0.749	0.178	0.056
	FWHM[a] (eV)	1.160	1.836	2.680	2.017	2.004
40 eV	Area	0.309	1.141	3.167	0.749	0.339
	FWHM (eV)	1.224	1.839	3.095	2.012	2.050

[a]FWHM = full width at half maximum.

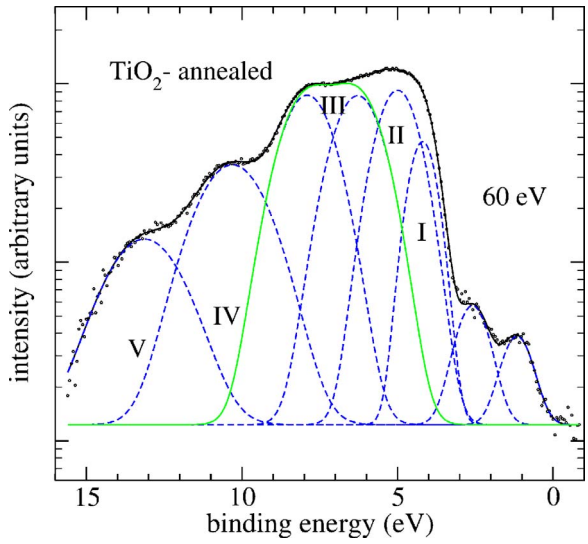

FIG. 5. UPS valence band spectra of annealed (800 °C) TiO_2 on a logarithmic scale. Six peaks are required to fit the main portion of the valence band. Two peaks take the place of peak III in Fig. 4.

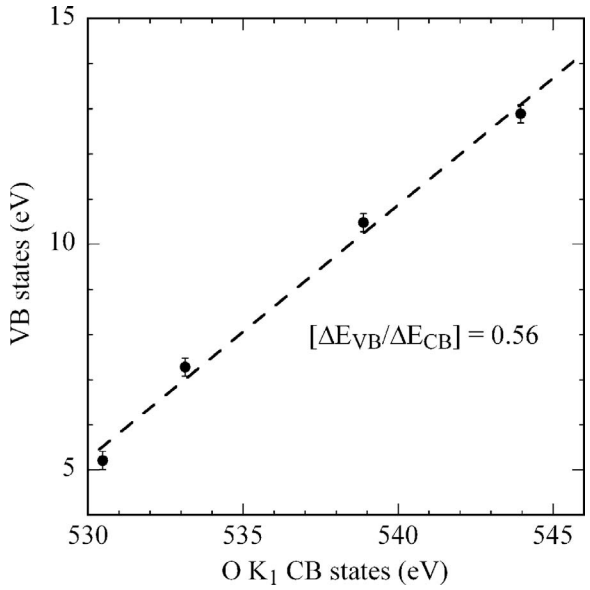

FIG. 7. Scaling of the TiO_2 valence band peak energies from UPS with the peak energies derived from the XAS data.

duction band. This contrasts with the behavior of the e_g levels in crystalline HfO_2, where the *d* states of e_g symmetry are π-bonded and lie higher in the valence band and lower in the conduction band. Complete removal of the remaining *d*-state degeneracies occurs with cooperative Jahn–Teller distortions along the *x*, *y*, and *z* axes. The understanding of these phenomena is grounded in the experimental evidence from XAS, UPS, photoconductivity measurements, and spectroscopic ellipsometry.[28]

A. XAS

Transitions in O K_1 x-ray absorption spectra are from the O 1*s* core level into the antibonding molecular orbitals of the conduction band. These levels are more purely atomic in character and more closely reflect the contributions from the transition metal atomic states than those of the valence band, which have a greater contribution from the O ligands.[29] Figure 6 is a molecular orbital diagram for Ti in an octahedral coordination with O atoms, included as a basis for interpretation of our results.[20] Though there are some differences in the literature about the ordering of the *s*- and *p*-derived a_{1g}

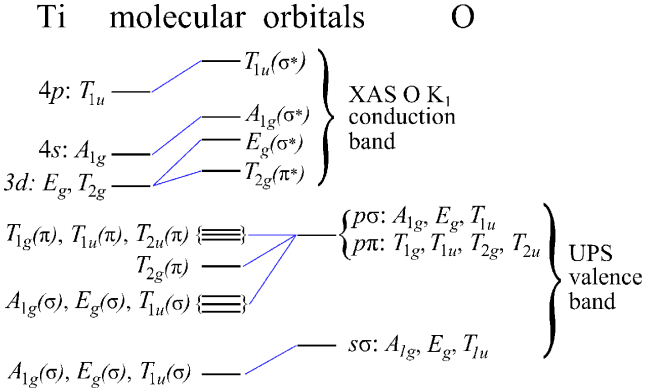

FIG. 6. The molecular orbital theory diagram for Ti and O atoms in an octahedral coordination, after Cotton (Ref. 20). This is used (see text) for interpreting the UPS spectra on TiO_2.

and t_{1u} states,[26,30–32] we follow the ordering presented in Cotton.[20] Hence, we assign the peaks I–IV in the TiO_2 O K_1 XAS spectrum of Fig. 1 as t_{2g}, e_g, a_{1g} [Ti 4*s*+O 2*p*(σ)-derived], and t_{1u} [Ti 4*p*+O 2*p*(π)-derived], respectively. Mixing among the Ti 4*s* and 4*p* states is expected to cause the structure of peaks III and IV. The local structure of group IVB oxides follows from the σ-bonded molecular orbitals and the symmetries of the underlying atomic states, especially those of the metal *d* electrons. For TiO_2, the *d* states with e_g symmetry form σ bonds with the O 2*p*, while those of t_{2g} symmetry form π bonds.

Complete removal of the *d*-state degeneracies has been distinctly observed in the Ti L_3 XAS spectrum [see Fig. 2(a)].[28] The average difference in the positions of the *d*-state t_{2g} and e_g contributions is about 2.8 eV. The energy separation is smaller than that in HfO_2, consistent with a greater crystal field splitting for 5*d* electrons compared to 3*d*, and also reflecting differences in the number of O-atom ligands, seven or eight for the 5*d* electrons in HfO_2, compared to six in TiO_2.[29] Further, t_{2g} and e_g *d* states are triply and doubly degenerate, respectively, and the five peaks form natural groupings of three and two, in qualitative agreement with the molecular orbital derivation of *d*-state materials with octahedral symmetry. These same features are present in the O K_1 absorption spectrum (Fig. 1) and though poorly resolved, are confirmed by the one-to-one correspondence with the Ti L_3 spectrum [see Fig. 2(b)].

Peaks III and IV of the O K_1 spectrum (the Ti 4*s* and 4*p* contributions) have energies more consistent with anatase than with rutile.[33] The shape of the L_3 spectrum in Fig. 2 is also more qualitatively similar to XAS spectra of anatase surfaces shown in the literature than it is to those of rutile.[7]

B. UPS

In UPS, the photoemission intensity depends on the total density of filled states and the transition probability or photoemission cross section. Valence band photoemission spec-

tra are frequently difficult to interpret, primarily because states are intrinsically broad, preventing the resolution of closely spaced states of different origins. In a crystalline material $E(k)$ dispersion must be taken into account. However, local structure is more important for transition metal oxides, and the importance of dispersion is somewhat lessened. The samples in this study are nanocrystalline, and so the data represent an average over the crystal orientations. The photoemission spectra of Fig. 3 have four visually apparent contributions, with a fifth revealed by the data analysis. This fifth peak, labeled I, represents the O $2p$ nonbonding states at the top of the valence band. It is important to note that final state effects are dominant for the valence band spectra and prevent a complete determination of symmetry assignments. The spectra actually represent a statistical sum over various distortions from the ideal octahedral structure. The molecular orbital diagram of Fig. 6 indicates that the σ-bonded d-derived states of e_g symmetry are initially degenerate with s- and p-derived states of a_{1g} and t_{1u} symmetry, respectively. Possible final state orderings of the spectral features associated with valence band molecular orbitals are given for undistorted octahedral molecules in Refs. 26 and 30–32. As an example, we have assigned peaks II through V as a mirror image of the conduction band states. In this case, the symmetry order is t_{2g}, e_g, a_{1g}, and t_{1u}, respectively. This would follow the "most probable" ordering of Bersuker[31] for octahedral complexes. Peak II is the π-bonded state primarily of Ti d-state and O $2p$-state character, while peaks III and IV are σ-bonded states. This assignment is given some credence through the linear scaling between the conduction band and valence band assignments, as shown in Fig. 7. The four states of the valence and conduction bands, t_{2g}, e_g, a_{1g}, and t_{1u}, are plotted with respect to each other showing a linear relationship with a slope of 0.56.

The Gaussian peaks in the fits of Fig. 3 are not intended to supply intrinsic linewidths. Single peaks have been used to represent the e_g and t_{2g} states, which show evidence of degeneracy removal in the XAS spectra. In the valence band, such state separations are entirely obscured by solid-state effects. However, the average separations can be extracted and are given in Table I in the column labeled Δd. The separation is 2.0 eV in TiO_2.

The UPS data acquired in this study were taken at photon energies of 40 and 60 eV, which are on opposite sides of a photoemission resonance at the Ti $3p \rightarrow 3d$ optical absorption edge at 47 eV.[5–7] Our valence band spectra show a much stronger intensity at 40 eV than 60 eV, as seen from Table II. A comparison to valence band spectra acquired on vacuum-annealed TiO_2 surfaces of anatase and rutile at photon energies of 40–80 eV would appear to reveal a stronger similarity to the resonance behavior of the anatase surfaces than to rutile, for which the Ti $3p \rightarrow 4sp$ resonance at 54 eV is dominant.[7] However, it is clear from the same study that the CIS spectra derived from the data are strongly influenced by sample preparation conditions and surface defect density, which makes any comparison to our nanocrystalline samples tenuous at best. Hence, the phase of the unannealed TiO_2 films cannot conclusively be identified as either anatase or rutile.

In Fig. 5, peak III of Figs. 3 and 4 has been replaced with two peaks. This additional peak was necessary to achieve an adequate fit and is evidence of an underlying Jahn–Teller splitting, as seen in the σ-antibonding states of the XAS data but unresolved in the UPS spectrum for the as-grown film. For the annealed films, which have larger crystallite sizes, these effects become noticeable even in the valence band data. It is likely that the films convert upon annealing to the anatase phase, which has a larger, more complex unit cell. The requirement of an additional Gaussian peak in fitting of the valence band is suggestive of such a transition. As discussed earlier, it is also more consistent with the features in the XAS data. The separation of the two replacement peaks in Fig. 5 is about 1.6 eV. The separation of the average position of these two states from the t_{2g} peak is 2.1 eV, similar to the $e_g - t_{2g}$ separation in the as-grown sample.

The band gap peaks of Fig. 4 are defect states attributable to oxygen vacancies. TiO_2 is an oxide with inherent oxygen vacancies most accurately described as $TiO_{2-\delta}$. The states have been chemically associated with Ti_2O_3 in studies of ion-bombarded surfaces of single-crystal TiO_2, and naturally trivalent oxides show the same intrinsic Ti 3+ state energies.[1,2] Oxygen vacancies result in partially filled Ti $3d$ nonbonding states within the band gap. As the Ti atoms remain in the local environment of the nanocrystallites, crystal field splitting and Jahn–Teller distortions are expected to affect the defect state energies. Hence, we observe two defect peaks near the valence band edge, a probable Jahn–Teller separation of a single Ti 3+ state of t_{2g} symmetry. These defects are the subject of a recent paper.[10]

V. CONCLUSIONS

The combined XAS and UPS study of TiO_2 films on silicon has revealed a correlation between the electronic structure of the conduction and valence bands and the molecular orbital model of octahedrally coordinated TiO_2. The XAS data show crystal field splitting and Jahn–Teller splitting corresponding to the octahedral bonding. In the valence band, the employment of a five-peak model based on molecular orbital theory was found to be suitable for fitting the data. Such a model is useful mainly for extracting the energies of valence band features for comparison to other samples and oxides, and for comparison to data from complementary spectroscopic measurements. Uncertainty concerning peak widths and the background subtraction limits some of its quantitative usefulness. However, the technique provided a systematic way of examining the valence band peaks, especially those of t_{2g} and e_g symmetry with mainly Ti $3d$–O $2p$ origin. Although some uncertainty remains as to the origin of the a_{1g} and t_{1u} σ bonding and antibonding states, it is observed that the valence band is contracted in energy with respect to the conduction band and on average may possess an inverse symmetry ordering.

Two features in the electronic structure indicated the unsuitability of pure TiO_2 for MOSFET gate dielectric applications. First, as has been determined elsewhere, the conduction band offset is ~0 eV. Second, intrinsic oxygen

vacancies result in defect states above the valence band edge. Though alloying of TiO_2 with other transition metal oxides may improve the conduction band offset, it is not expected to remove the bandgap defects.

[1]V. E. Henrich, G. Dresselhaus, and H. J. Zeiger, Phys. Rev. Lett. **36**, 1335 (1976).
[2]R. H. Tait and R. V. Kasowski, Phys. Rev. B **20**, 5178 (1979).
[3]U. Diebold, Surf. Sci. Rep. **48**, 53 (2003).
[4]J. G. Chen, Surf. Sci. Rep. **30**, 1 (1997).
[5]E. Bertel, R. Stockbauer, and T. E. Madey, Surf. Sci. **141**, 355 (1984).
[6]Z. Zhang, S.-P. Jeng, and V. E. Henrich, Phys. Rev. B **43**, 12004 (1991).
[7]A. G. Thomas, W. R. Flavell, A. K. Mallick, A. R. Kumarasinghe, D. Tsoutsou, N. Khan, C. Chatwin, S. Rayner, G. C. Smith, R. L. Stockbauer, S. Warren, T. K. Johal, S. Patel, D. Holland, A. Taleb, and F. Wiame, Phys. Rev. B **75**, 035105 (2007).
[8]M. Houssa and M. M. Heyns, in *High-κ Gate Dielectrics*, edited by M. Houssa (IOP Publishing, Bristol, 2004).
[9]G. D. Wilk, R. M. Wallace, and J. M. Anthony, J. Appl. Phys. **89**, 5243 (2001).
[10]G. Lucovsky, H. Seo, S. Lee, L. B. Fleming, M. D. Ulrich, J. Lüning, P. Lysaght, and G. Bersuker, Jpn. J. Appl. Phys., Part 1 **46**, 1899 (2007).
[11]S. Lee, G. Lucovsky, and J. Lüning, J. Vac. Sci. Technol. B (2007) (submitted).
[12]D. A. Neumayer and E. Cartier, J. Appl. Phys. **90**, 1801 (2001).
[13]G. B. Rayner, Jr., D. Kang, and G. Lucovsky, J. Vac. Sci. Technol. B **21**, 1783 (2003).
[14]D. T. Cromer and K. Herrington, J. Am. Chem. Soc. **77**, 4708 (1955).
[15]V. W. H. Baur, Acta Crystallogr. **9**, 515 (1956).
[16]M. E. Straumanis, T. Ejima, and W. J. James, Acta Crystallogr. **14**, 493 (1961).
[17]L. A. Grunes, Phys. Rev. B **27**, 2111 (1983).
[18]G. van der Laan, Phys. Rev. B **41**, 12366 (1990).
[19]J. C. Woicik, E. J. Nelson, L. Kronik, M. Jain, J. R. Chelikowsky, D. Heskett, L. E. Berman, and G. S. Herman, Phys. Rev. Lett. **89**, 077401 (2002).
[20]F. A. Cotton, *Chemical Applications of Group Theory*, 2nd ed. (Wiley-Interscience, New York, 1971).
[21]L. Fleming, M. D. Ulrich, and J. E. Rowe (unpublished).
[22]L. Fleming, C. C. Fulton, M. D. Ulrich, G. Lucovsky, and J. E. Rowe (in preparation).
[23]S. Sayan, E. Garfunkel, and S. Suzer, Appl. Phys. Lett. **80**, 2135 (2002).
[24]C. C. Fulton, G. Lucovsky, and R. J. Nemanich, J. Vac. Sci. Technol. B **20**, 1726 (2002).
[25]J.-J. Yeh, *Atomic Calculations of Photoionization Cross Sections and Asymmetry Parameters* (Gordon and Breach, Langhorne, PA, 1993).
[26]P. A. Cox, *Transition Metal Oxides* (Oxford University Press, New York, 1992).
[27]C. Sousa and F. Illas, Phys. Rev. B **50**, 13974 (1994).
[28]G. Lucovsky, C. C. Fulton, Y. Zhang, Y. Zou, J. Luning, L. F. Edge, J. L. Whitten, R. J. Nemanich, H. Ade, D. G. Schlom, V. V. Afanase'v, A. Stesmans, S. Zollner, D. Triyoso, and B. R. Rogers, IEEE Trans. Device Mater. Reliab. **5**, 65 (2005).
[29]H. B. Gray, *Chemical Bonds: An Introduction to Atomic and Molecular Structure* (University Science Books, Mill Valley, CA, 1994).
[30]C. J. Ballhausen and H. B. Gray, *Molecular Orbital Theory* (W. A. Benjamin, New York, 1965).
[31]I. B. Bersuker, *Electronic Structure and Properties of Transition Metal Compounds* (John Wiley & Sons, New York, 1996).
[32]G. Lucovsky and J. L. Whitten, in *High Dielectric Constant Materials*, edited by H. R. Huff and D. C. Gilmer (Springer, New York, 2005).
[33]V. S. Lusvardi, M. A. Barteau, J. G. Chen, J. Eng, B. Frühberger, and A. Teplyakov, Surf. Sci. **397**, 237 (1998).